ARAIM Operational Performance Tested in Flight

Markus Rippl[1], Ilaria Martini[1], Boubeker Belabbas[1], Michael Meurer[1,2]
[1]Institute of Communications and Navigation, German Aerospace Center (DLR), Oberpfaffenhofen, Germany
[2]Institute of Navigation, RWTH Aachen University, Germany

BIOGRAPHIES

Markus Rippl received his Diploma in Electrical Engineering and Information Technology from Technische Universität München (TUM) in 2007. Since then, he has been a research associate with the Institute of Communications and Navigation (IKN) at the German Aerospace Center (DLR) in Oberpfaffenhofen near Munich. His areas of interest include GNSS integrity using receiver-side algorithms, next generation Receiver Autonomous Integrity Monitoring (RAIM) algorithms and architectures, and the development of a future integrity architecture supporting Advanced Receiver Autonomous Integrity Monitoring (ARAIM) with an Integrity Support Message (ISM).

Ilaria Martini received the Master Degree in telecommunication engineering and the Ph.D. in information technology from the University of Florence, Italy. She was at the Galileo Project Office of ESA/ESTEC in 2003, working on the performance of the Galileo Integrity Processing Facility. She was research associate in 2004 at the University of Florence and in 2005 at the Institute of Geodesy and Navigation of the Federal Armed Forces Germany in Munich. In 2006 she joined the navigation project department of Ifen GmbH in Munich. Since 2012 she works as research associate in the Institute of Communication and Navigation at the German Aerospace Center (DLR), Oberpfaffenhofen. Her main area of interest is GNSS Integrity Monitoring.

Boubeker Belabbas obtained an MSc. Degree in Mechanical Engineering from ENSEM in Nancy (France) and a specialized MSc. Degree in Aerospace Mechanics from Supaero in Toulouse (France). He joined DLR in 2001 and developed the Navigation Integrity activities. He is now leading the GNSS integrity team in the Department of Navigation of the Institute of Communications and Navigation.

Michael Meurer received the diploma in electrical engineering and the Ph.D. degree from the University of Kaiserslautern, Germany. After graduation, he joined the Research Group for Radio Communications at the Technical University of Kaiserslautern, Germany, as a senior key researcher, where he was involved in various international and national projects in the field of communications and navigation both as project coordinator and as technical contributor. From 2003 till 2013, Dr. Meurer was active as a senior lecturer and Associate Professor (PD) at the same university. Since 2006 Dr. Meurer is with the German Aerospace Centre (DLR), Institute of Communications and Navigation, where he is the director of the Department of Navigation and of the center of excellence for satellite navigation. In addition, since 2013 he is a professor of electrical engineering and director of the Institute of Navigation at the RWTH Aachen University. His current research interests include GNSS signals, GNSS receivers, interference and spoofing mitigation and navigation for safety-critical applications.

ABSTRACT

This paper presents a flight performance analysis of next-generation ARAIM based on GPS and GLONASS dual-frequency data collected during flight trials using DLR's research aircraft ATTAS. The test results are based on joint PVT and ARAIM post-processing and investigate potential differences between simulated ARAIM performance levels and actual operational performance. The PVT and ARAIM performance is evaluated with respect to positioning accuracy, position error bounding (integrity) and availability of LPV200 (Localizer Performance with Vertical Guidance) service during typical arrival and approach maneuvers. This evaluation takes into account operational constraints such as signal outages due to banking. These constraints are not included in analyzes based on static user grids with fixed elevation masks and thus constitute the characteristic feature of this study. To ensure that the performance metrics obtained can be compared with performance simulation results, the error model targeted at future GNSS with L1 and L5 signals is adapted to represent the error model for the data collected, L1 and L2.

Compliance with integrity requirements is demonstrated conditioned on a fault-free scenario, which is ensured by post-processing and analyzing the airborne data together with ground reference data. Flight test results are compared with results from a predictive study that estimates ARAIM performance with a simulation for a static user in the vicinity of the airport. The comparability of these results is made possible by adjusting the dual frequency user range error model to the scenario at hand and applying the same SIS error parameters both to the real-data ARAIM processing chain and the simulated scenario.

I. INTRODUCTION

The next years will bring an ever increasing number of ranging signals for users of Global Navigation Satellite Systems (GNSS), many of them being freely available at two frequency bands and using modernized modulation with better performance than today. Not only will aviation users be able to obtain better positioning accuracy in this new era of GNSS operations, but more importantly this will enable

navigation solutions for more demanding applications like precision approach. The Advanced Receiver Autonomous Integrity Monitoring (ARAIM) algorithm is a key technology to introduce stand-alone airborne navigation for critical phases of flight without requiring augmentation systems such as SBAS or GBAS (Satellite, or Ground Based Augmentation Systems). It satisfies the demand for integrity services that provide robustness against multiple simultaneous satellite faults, and at the same time it can make the best possible use of this multitude of emerging modernized GNSS signals, resulting in highly robust navigation services spanning the applications from en-route to precision approach at surpassing availability.

ARAIM was introduced in [11, 4] and originates from [20]. It is a RAIM method capable of obtaining navigation integrity for stand-alone users and was designed to exploit the high number and quality of GNSS signals that will be available in the future: Multiple GNSS constellations, providing L1 and L5 signals that make dual frequency measurements also available for users of the aviation community. As opposed to classical weighted least square RAIM [25] it complies with more stringent integrity requirements that are mandatory for aircraft precision approach. The most remarkable improvement is its ability to bound position errors (i.e. protection levels) under nominal, single and multiple fault conditions. It is expected that upon the availability of next-generation GNSS signals from GPS, Galileo, GLONASS and Compass, the worldwide integrity performance using ARAIM will be sufficient to provide LPV-200 navigation capability without the need of conventional augmentation systems such as WAAS or EGNOS [22, 6]. The standardization of ARAIM and the underlying assumptions have been discussed in [12, 13], and more recently further directed towards the definition of a suitable ground architecture for a "light" integrity support message (ISM) in [2, 3]. It is already foreseeable that together with the desirable leap in terms of navigation performance, the transition from RAIM to ARAIM will also increase complexity of the ground architecture and user algorithm.

The expected level of performance for future ARAIM users has been thoroughly discussed in various studies during the past years [22, 8, 12] . Most investigations estimate the availability of ARAIM with respect to its performance parameters Vertical Protection Level (VPL), Effective Monitoring Threshold (EMT) and vertical accuracy. The results are obtained by simulation of static user grids and multiple full constellations, e.g. GPS and Galileo. Furthermore, these simulations assume available ranging signals on L1 and L5, and generally, the existence of multiple modernized GNSS constellations with better orbit and clock performance than today.

In these cases ARAIM is analyzed without consideration of the positioning performance, particularly its limitation caused by operational constraints such as signal loss, cycle slips, and other effects. While this approach is suitable to compare performance of candidate ARAIM architectures it must be confirmed whether the operational performance on board an aircraft can be adequately assessed with such an analysis. When compared with classical Least-Squares RAIM methods it can be observed that ARAIM is more susceptible to small geometries. This effect results from the inclusion of reduced geometries into the computation of the error bound VPL.

At the same time, due to the projected increase of traffic in civil aviation, effort is put into finding new approach patterns that can increase efficiency on the runways. The primary target for these activities is to allow more aircraft landings and departures per hour. Possible solutions to this problem include flexible routing schemes in the arrival phase, with a late turn-to-final and potentially more frequent turns in general. Continuous Descent Approach (CDA) patterns are discussed as a means to reduce fuel costs, and to reduce aircraft noise. In summary, these potential changes to the aspects of landing operations can also change the availability of ARAIM based navigation, and the aforementioned grid simulations do neither reflect current operational aspects nor potential changes in the future. For the aviation community it is therefore interesting to look at performance studies that can relate the predicted future ARAIM performance levels to actual in-flight scenarios with all their restrictions.

The German Aerospace Center (DLR) executed a series of flight trials using its Research Aircraft ATTAS, a VfW 614 medium sized jet aircraft. The purpose of this flight trial series was to demonstrate novel means of navigation for precision approach while at the same time analyzing the feasibility of next generation arrival procedures with modernized Flight Management Systems (FMS) and Air Traffic Control (ATC) systems. A GNSS receiver on board the aircraft was used to record measurement data on two frequencies from GPS and GLONASS during these flights. In addition, a set of ground reference receivers located at the airport premises provides additional data that was used to compute an RTK-based reference trajectory. Furthermore, a position and attitude reference was being recorded with a combined GPS/INS reference system at a high data rate.

This paper presents flight test results based on joint PVT and ARAIM post-processing and investigates potential differences between simulated ARAIM performance levels and actual operational performance. The PVT and ARAIM performance is evaluated with respect to positioning accuracy, robust position error overbounding (integrity) and availability of LPV-200 service during typical arrival and approach maneuvers. The evaluation takes into account actual operational constraints such as signal outages due to banking, effects that are not included in studies based on static user grids with fixed elevation masks. Compliance with integrity requirements is demonstrated conditioned on a fault-free scenario, which is ensured by post-processing and analyzing the airborne data together with ground reference data.

Two properties of a user scenario have large impact on the ARAIM performance: The user geometry, i.e. the number and position of the satellites with respect to the user, and the model parameters that define the portion of the user range error that can not be corrected. To ensure that results derived from the flight test can be compared to ARAIM performance

predictions the user range error models are adapted to the scenario of the flight trials. This adaptation includes changing the error model due to different modulation and signal reception techniques applying for GPS L2 semi-codeless tracked signals and GLONASS signals in general. Furthermore, the ephemeris and clock error assumptions for future GNSS systems have been reviewed and changed to match the performance of today's constellations.

The results obtained from processing dual-frequency GPS and GLONASS measurements collected in a test flight are then compared with theoretical results that apply the same model assumptions. The discrepancy between these results demonstrates how operational performance differs from the predicted performance of previous theoretical studies and isolates its cause: A GNSS receivers in an airborne environment has to cope with more frequent outages of satellite signals due to blocking or weak signal strength, and this effect can dominate the performance of an ARAIM algorithm especially while maneuvers in the approach and landing phase are executed.

This paper is structured as follows. In the following Section II, the details of the used position and integrity algorithms are described. Section III defines the user range error applied to both the theoretical and data-derived ARAIM computations presented throughout the paper. It shows the alterations to the existing L1/L5 model that are necessary to match the properties of currently available GNSS and the specific set of range measurements that have been collected, i.e. semi-codeless tracking range measurements for GPS, and the use of GLONASS as a second constellation. Then Section IV applies these derived model parameters to a theoretical analysis of ARAIM availability and discusses the results of this simulation. In Section V the data collected during the flight tests is processed and analyzed. We also compare the performance levels obtained from theory and data, and discuss the corresponding effects that cause the discrepancy. Section VI discusses the higher level consequences from the findings in this paper.

II. PVT and ARAIM Processing

A. Data Preprocessing and Position Computation

The measurements used in this paper originate from a GNSS receiver operated on board DLR's research aircraft ATTAS (Figure 1). The antenna is placed approximately in the middle of the fuselage above the cabin. The receiver is a geodetic TOPCON NetG3 receiver, where the loop bandwidths and receiver settings have been configured to provide good tracking even in the high dynamic environment of the aircraft. The measurements were stored on the equipment and later extracted to RINEX format for post-processing.

An additional GPS/INS reference system provides attitude and position, but no range measurements. This data is however logged to the on-board experimentation equipment and can later be retrieved and taken into account for post-processing. Furthermore the reading of a radar altimeter is also logged continuously.

Figure 1. DLR's former VfW 614 research aircraft ATTAS (retired 2012)

Apart from airborne measurements we also recorded ground reference data from three GNSS receivers set up at the airport. These receivers are normally used for an experimental GBAS set-up, but the data can be used to obtain an RTK solution of the on-board receiver, serving as a precise position reference. However the ground receivers had been recording only L1 and L2 signals of the GPS constellation, so no GLONASS reference data was available. Data from the nearby IGS station POTS (Potsdam, Germany) was thus processed in order to analyze the GLONASS signals with a known reference position. This station is one out of only a few in the vicinity of the flight test providing GLONASS data available for the day of the flight test.

The flight FE04 was recorded on Nov. 04, 2011 and included several approaches to runway 08 of the Braunschweig research airport EDVE (Figure 2). In addition to the approaches several full circles were executed in order to test various telemetry equipment during the level segments at FL 120. For the present study these maneuvers are useful to understand the consequences of large banking angles on the PVT and Integrity solution.

The position estimates and corresponding integrity data are generated in a post-processing software implemented in MATLAB. After parsing the RINEX data the software generates a data base of available ephemeris from the RINEX NAV files. It then proceeds to read the range and phase measurements epoch by epoch at an input interval of 0.5 seconds. From all satellites with available L1 and L2 measurements an ionosphere free linear combination is computed for code and for carrier. These are then fed into a hatch filter module which performs code-minus-carrier smoothing [24]. If a measurement is missing the filter is reset for the corresponding satellite channel. The filter time constant is set to 100s, and the measurements are accepted only for further processing after the filter has converged. Following [24] it can be assumed that this is the case after 360s for the suggested filter. In this work, we use this waiting time as a standard value, but show also the

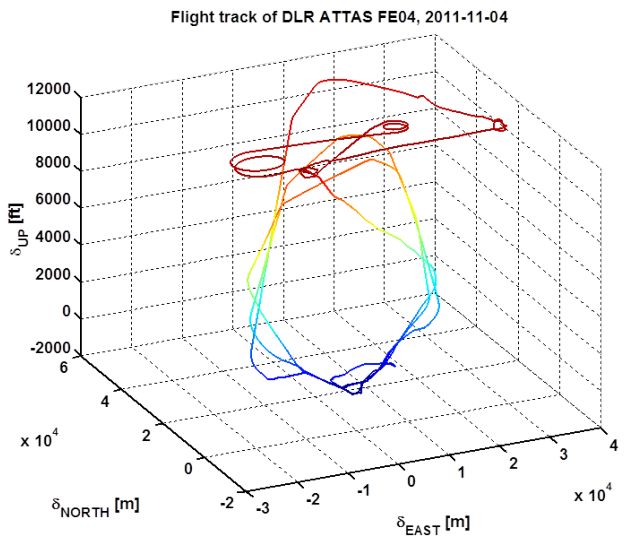

Figure 2. Flight track of FE04, centered around ARP of Braunschweig Research airport (EDVE)

performance assuming a shorter filter setup time of only 20s to highlight the impact of outages in combination with long filter convergence times.

The user position is estimated using a weighted least squares iterative approach. No known time offset between the GPS and GLONASS system times is assumed, therefore the algorithm solves for five unknowns whenever range measurements from more than one GNSS are present. Weighting of the pseudorange measurements needs to be in line with the assumptions used in the MHSS algorithm to compute the Protection Levels. Both modules are therefore connected with the same error model that generates user range corrections and standard deviations of the user range error and of the residual errors after correcting effects such as the troposphere. The error model and its parametrization are further described in Section III.

B. Advanced Receiver Autonomous Integrity Monitoring with MHSS

The ARAIM algorithm adopted to obtain navigation integrity is based on the multiple hypothesis technique [20] which was extended during the past years to MHSS based RAIM [5], targeting to fulfill the integrity requirements for precision approach [17]. The version of the MHSS ARAIM algorithm used throughout this work includes an optimized allocation of the integrity budget into MHSS hypotheses [4] and the extensions discussed in the ARAIM-Technical Subgroup of the Working Group C [2]. A complete and accurate definition of the MHSS algorithm version used within this study is available in [7]. With respect to our previous work [21] the computation of fault free VPL and EMT have changed, and a second fault monitor based on a χ^2 hypothesis test was added to FDE capabilities.

ARAIM employs a multiple hypothesis approach to incorporate the potential effects of single or multiple satellite faults into its prediction of the worst case error, the Protection Level (PL). Any combination of faults is first evaluated with respect to its prior probability of occurrence. If a fault mode (i.e., one unique combination of faulted and healthy measurements) is likely to occur, a subset of measurements excluding the potential fault candidates is established and a subset based position is estimated. With all hypothetical position solutions merged into a union of position estimates it is possible to state the probability that the resulting interval contains at least one position solution based entirely on fault free measurements. The remaining fault hypotheses which were not considered in the interval constitute the set of unmonitored hypotheses. The set of these hypotheses is chosen such that the sum of their probabilities is a fraction of the permitted integrity budget. For LPV-200 approaches, this overall integrity risk is defined as $P_{HMI} = 2 \cdot 10^{-7}$. Because MHSS does not make a decision with respect to the fault states of the satellites involved in computing a position solution, every position solution with integrity "contains" reduced subset geometries. Thus this algorithm is much more susceptible to geometry size than classic RAIM [25]. This property motivates the following analysis of the effects that signal loss during flight may have on ARAIM operational performance.

III. Definition of the User Range Error Model

This section defines the user range error model that is applied within both the position computation algorithm and the MHSS ARAIM integrity computation. It covers the estimation of parameters that accurately describes the user range error distribution for the particular flight test data, and derives its generation from the more optimistic L1/L5 dual frequency error model currently assumed for future ARAIM operations after modernization and full deployment of Galileo and GPS [2].

The importance of an accurate error model can be seen from looking at the MHSS protection level equation (1) for optimized integrity risk allocation,

$$2Q\left(\frac{\mathrm{VPL}-b_3^{(0)}}{\sigma_3^{(0)}}\right)+\sum_{k=1}^{N_{\text{fault modes}}} P_{\text{fault,k}}\,Q\left(\frac{\mathrm{VPL}-T_{k,3}-b_3^{(k)}}{\sigma_3^{(k)}}\right)= \\ = P_{\text{HMI}}-P_{\text{not monitored}} \tag{1}$$

where $P = Q(x)$ is the one-sided tail probability of a Gaussian distribution at x, $b_3^{(k)}$ is the worst-case bias of the vertical solution k taking into account all maximum biases from the satellite measurements included in the solution. $\sigma_3^{(k)}$ is the vertical position accuracy, based on overbounded distributions (URA). $P_{\text{fault,k}}$ is the prior likelihood of occurrence for the fault mode k. $T_{k,3}$ is the threshold of the FDE test that compares the estimate of a solution separation with its actual value, based on range residuals. P_{HMI} is the total available integrity risk for the vertical error bound, and $P_{\text{not monitored}}$ is a partition of the risk that is directly allocated to failure modes $k_{\text{NM}} \notin N_{\text{fault modes}}$.

From (1) it follows:

- The integrity budget is split across all possible combinations of faulted/non faulted satellites, where the less likely cases are directly accounted for without computation of a partial VPL, and for the likelier fault modes we compute a VPL
- VPL is a function of the allocated budget for each fault mode such that the resulting VPLs for each mode are equal. This method is the optimization described in [4].
- The VPL for each fault mode k depends on the vertical accuracy of the respective solution, $\sigma_3^{(k)}$, and the magnitude of the bias components that are summarized in each $b_3^{(k)}$.

The vertical accuracy $\sigma_3^{(k)}$ is derived from assumed variances of the respective error contributions to the ranges that are used in each fault mode k. If the error model is too conservative, the VPL will be higher than necessary to overbound the position error at the required integrity risk. If the error model is too optimistic however, the position error is not overbounded by the VPL at the allocated probability. Of course the same holds for any mismodeling of the bias components that are defined in the error model.

In the frame of this study, the amount of range measurements is too small to allow for a statistically meaningful proof of integrity with respect to this overbound. If the error model was too optimistic, the resulting VPLs and vertical errors would not necessarily show this flaw. Still the derived level of performance would be better than with an accurate model. This consideration motivates the careful adaptation of the user range error model to this specific L1/L2 scenario.

A. Contributions to the UERE Budget

With respect to user position accuracy, the relevant quantity for each satellite range measurement can be denoted

$$\delta\rho^{(i)} = \left(\rho^{(i)} - \text{corrections}^{(i)}\right) - \left\|x^{(i)} - x_u\right\| \ , \qquad (2)$$

where $\rho^{(i)}$ is the actual range measurement including all errors and by *corrections* we denote the sum of all range measurement corrections that are applied to this measurement based on a model. The geometric distance between the user x_u and the satellite $x^{(i)}$ is defined by $\left\|x^{(i)} - x_u\right\|$.

Because the error of the modeled, or expected range is the targeted parameter rather than the measurement error, we denote the parameter of interest, $\delta\rho_k$, as the *User Equivalent Range Error*, or UERE in the following. Furthermore it is important to state that this error budget applies to nominal errors only - a non-nominal error as defined in the fault modes k of the MHSS algorithm is defined with an unlimited bias magnitude.

Table I is a summary of all errors that contribute to the nominal UERE budget. For each error origin, the corresponding parameter in the original dual frequency range error model [2] is given. The necessary changes with respect to the GPS L1/L2 model and the GLONASS model are then described in the following columns. In the following subsection we first detail the error model for L1/L5 dual frequency users of GPS and Galileo.

B. L1-L5 GPS-Galileo Model

The error model for non-differential airborne GNSS users in a dual frequency scenario using GPS and Galileo can be based on the assumptions defined in [2], Annex B. These values and equations were used as a baseline for multiple performance simulations executed in the WG-C ARAIM Subgroup. Whereas the Galileo user multipath and tracking noise variances were defined in tabular form, the GPS model follows the Airborne Accuracy Designator (AAD) definition in [23, 19]. Both GNSS constellations assume the same tropospheric correction model with the variance of the residual troposphere error defined as in [24].

1) Orbit and clock errors: The discrepancy of the satellite's true position on orbit at a given time and the position computation derived from its broadcast orbit, and the difference between the true SV clock offset and the broadcast offset given as a third order polynomial. Two models exist to describe this error for future ARAIM users: The first, *User Range Accuracy* (URA) for GPS or *Signal in Space Accuracy* (SISA) for Galileo is a Gaussian overbound that corresponds to the worst case user projection of any combination of the three-dimensional orbit errors and the error of the modeled SV clock offset. GPS and Galileo broadcast URA/SISA values in the navigation message. The parameter depends heavily on the methodology and quality of orbit determination and time synchronization (ODTS) performed by the GNSS operator's ground processing facility, and its accurate estimation requires good observability of the orbit/clock states of all satellites at all times as well as a long enough observation history. The assumed values in [2] are 0.75m for URA and 0.957m for SISA. In contrast, the broadcast URA values in GPS today have been found to range between 2m and higher values for the flight test data that has been processed.

The second model describes an expected value of the error and is called *User Range Error* (URE) for GPS, or *Signal in Space Error* (SISE) for Galileo. The use of this parameter in MHSS ARAIM is to provide an accurate expectation of the position error in cases where no conservatism at integrity level is needed, in particular to compute the expected difference between two solutions based on different subsets (Solution Separation). URE values are obviously smaller because they reflect less conservatism, and the corresponding values in [2] are 0.5m (URE) and 0.67m (SISE).

2) Nominal signal deformation, inter-frequency biases and phase center variations of the SV antenna: These three error contributions are modeled as a bias since they represent effects that are mostly stationary, considering the limited time frame of an ARAIM operation (Approach time 150s). The same distinction regarding the application of the respective parameter is made as with URA/URE: A maximal bias is denoted B_{int}, where the values for GPS and Galileo have been assumed at 0.75 and 1.00m. An expected bias B_{cont} is modeled

Nominal Error	L1/L5	GPS L1/L2 P(Y)	GLONASS L1/L2
Orbit/Clock	URA/URE, SISA/SISE	Verify	Verify
Signal Deform., PCV & IFB	B_{int}, B_{cont}	Verify	Verify
Ionosphere	Mitigated (1st order)	Ident.	Ident.
Troposphere	MOPS model [1]	Ident.	Ident.
Multipath	Gaussian Overbound	Adapt	Adapt
Code Tracking	Gaussian	Adapt	Adapt
RX biases	Compensated	Ident.	Ident.
Multipath Smoothing	Factor	Verify	Verify
Ifree Linear Combination	Frequency dependent factor	Adapt	Adapt

Table I
UERE BUDGET FOR L1/L5 AND THE L1/L2 SCENARIOS AT HAND

for continuity purposes. In the cited assumptions document this value has been assumed zero for both constellations.

3) Ionosphere Error: In a dual frequency scenario, the first order ionosphere delay is removed from the range measurements by forming a ionosphere free linear combination of each pair of measurements. The higher order ionosphere errors remain unmodeled, but its magnitude is in the millimeter range [14] and thus can be neglected for positioning applications based on code measurements.

4) Troposphere Error: In contrast to the ionosphere, the delay of the troposphere is not frequency dependent and thus can not be resolved by using dual frequency measurements. The MOPS troposphere model provides both an estimate for the tropospheric propagation delay and an estimated variance of the residual troposphere error after its correction [24]:

$$\sigma_{\text{tropo}}(\theta) = 0.12m \cdot \frac{1.001}{\sqrt{0.002001 + sin^2(\theta)}} \tag{3}$$

As an purely elevation dependent model, no difference exists between its application to GPS and Galileo measurements.

5) Receiver Multipath: For aviation users the airborne multipath is assumed as white noise primarily originating from reflections at wings and fuselage. Due to the high dynamics of aircraft, only little stationary multipath components affect the user. The standard deviation of the multipath error distribution at user receiver level is defined as an elevation dependent quantity [24]

$$\sigma_{\text{multipath}}(\theta) = \left(0.13 + 0.53 \cdot e^{-\theta[deg]/10[deg]}\right) \text{[m]} \tag{4}$$

The impact of multipath on code- and carrier measurements however depends heavily on the modulation of the corresponding signals. The model at hand is originally defined for single frequency GPS users, but in this case it is also applied for the L5 signal. As mentioned before the assumptions document defines a multipath and noise function given in tabular form that does not fully correspond to the MOPS model denoted here.

6) Receiver tracking noise: The code tracking noise defined in [24] includes receiver noise, thermal noise, interference, inter-channel biases, time since smoothing filter initialization and processing errors. A model based on a Gaussian distribution with standard deviation for users with an Airborne Accuracy Designator (AAD) A is referenced:

$$\sigma_{\text{noise}}(\theta) = \left(0.15 + 0.43 \cdot e^{-\theta[deg]/6.9[deg]}\right) \text{[m]} \tag{5}$$

Again, as it can be seen in the model derivation [19], these values depend a lot on the signal properties, in particular the modulation, signal strength and receiver configuration such as loop bandwith and correlator spacing. Special attention has to be paid for cases such as the semi-codeless tracking for GPS L2 P(Y), and also for GLONASS signals in general.

7) Receiver biases: Large biases at receiver level, e.g. inter-channel biases, have to be compensated or accounted for by the variance of the receiver tracking noise [24]. Thus they are not explicitly considered in this UERE budget.

8) Code-Carrier Smoothing effect on multipath: The code-carrier smoothing filter [24] reduces code measurement noise that is uncorrelated and zero mean with respect to the filtering time constant. The analysis in [9] assumes a constant α applied to the MOPS [24] Multipath model,

$$\sigma_{\text{multipath}} = \alpha \cdot \left(0.13 + 0.53 \cdot e^{-\theta[deg]/10[deg]}\right) \text{[m]} \; . \tag{6}$$

In general, multipath on the airborne user antenna is considered as a high dynamic, non-stationary effect where this assumption holds. However in this work we neglect this effect and instead adopt the more conservative assumption of the MOPS multipath.

9) Ionosphere free combination: The linear combination of two code measurements at frequencies f_1, f_2 has increased multipath and tracking noise [9]:

$$\sigma_{\text{usr,f1f2}} = \sqrt{\left(\frac{f_1^2}{f_1^2 - f_2^2}\right)^2 \sigma_{f1}^2 + \left(\frac{f_2^2}{f_1^2 - f_2^2}\right)^2 \sigma_{f2}^2} \; , \tag{7}$$

where the single-frequency tracking and multipath noise follows from

$$\sigma_{fi}^2 = \sigma_{\text{noise},i}^2 + \sigma_{\text{multipath},i}^2 \quad . \tag{8}$$

If identical receiver and multipath noise levels are assumed, the equation can be simplified to [2]

$$\sigma_{\text{usr,f1f2}} = \sqrt{\frac{f_1^4 + f_2^4}{\left(f_1^2 - f_2^2\right)^2}} \cdot \sqrt{\sigma_{\text{noise}}^2 + \sigma_{\text{multipath}}^2} \tag{9}$$

This concludes the definition of the baseline L1/L5 UERE model, which will now be adapted to match the L1/L2 signals received during the flight test.

C. L1-L2 GPS-GLONASS Model

This section covers alterations to the above described model so that the parameters accurately represent the properties of L1 and L2 signals. Following Table I, the following differences require special attention:

- The broadcast URA of today's GPS signals suggests that the rather strict assumption of 0.75m can not be safely assumed.
- The accuracy specifications of GLONASS ephemerides [15, Table 4.2] are significantly wider than the URA/SISA assumptions, and no information concerning the interpretation of these figures with respect to overbounding is given.
- Signal deformation and inter-frequency biases depend on the satellite payload and modulation details.
- Receiver level multipath and tracking noise depend on the signal modulation scheme, signal strength, and lastly on the receiver configuration.
- The noise level increase due to the ionosphere free combination depends on the ratio of the two frequencies involved.

On the other hand some of the error contributions for L1/L2 signals can safely be assumed identical to the models described above. These include

- The residual ionosphere error which is considered negligible for the application at hand.
- The residual troposphere error, which is an elevation dependent quantity and neither frequency dependent nor connected with signal properties
- The reduction of multipath and tracking noise due to code-carrier smoothing, which can be approximated as a function of the smoothing time.

In the following we describe what steps are taken to adapt the model parameters:

1) Orbit and clock errors: In the GPS case it seems reasonable to assume that the broadcast URA values robustly overbound the worst-case user range error caused by ephemeris and clock state imprecision. To validate this assumption the orbit errors were estimated for the day in question. The "true" satellite position is computed using post processed precise orbits (SP3). Figures 3 and 4 indicate the ECEF orbital errors of two GPS satellites (PRN 05 and 06), derived from the difference between broadcast and SP3 precise ephemerides. In Figure 4 it can be seen that at midday an ephemeris transition causes a jump in the Y-axis that is rather large. However the broadcast URA reflects this decrease of performance, so it seems justifiable to accept the broadcast values for GPS.

No URA value is accessible through RINEX data for GLONASS orbits, so an estimate of URA values that can be used in this study is directly made from analyzing the orbit errors. Figures 5 and 6 represent these in the ECEF frame. The broadcast satellite position is derived from an integration of the equations of motion parametrized by the broadcast satellite states. The reference positions are interpolated from a precise SP3 reference downloaded from IGS. Figure 5 is an example

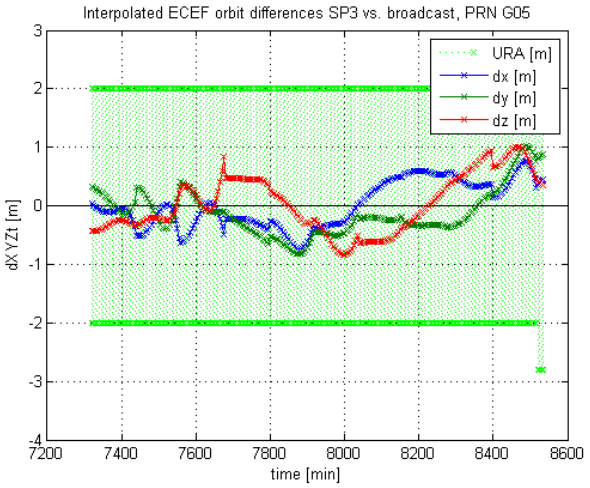

Figure 3. Orbit errors of GPS PRN 05

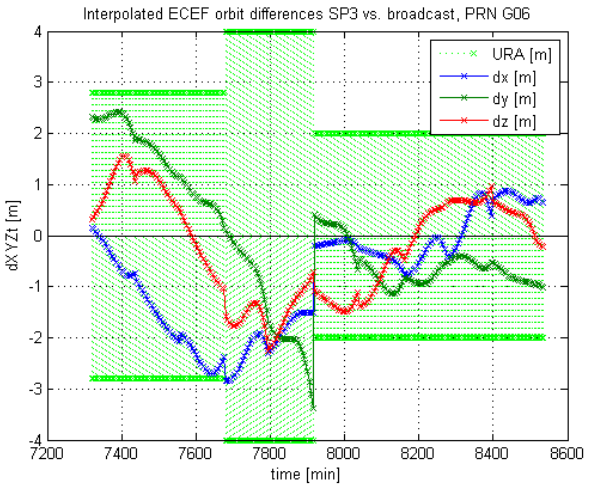

Figure 4. Orbit errors of GPS PRN 06

of a "good" satellite found in the data set; whereas Figure 6 can be considered as a worst case example (related to the one day data that was processed).

In both cases the magnitude of the orbital errors seems larger than in the GPS examples, but it can also be seen that the errors are sinusoidally formed with a frequency that can be related to the orbital period of the spacecraft. Two possible causes for this periodic error are suggested:

First, the two ephemerides refer to different locations on the satellite: The broadcast orbit describes the position of the phase center of the antenna, and the SP3 data describes the center of mass position in orbit for all GLONASS satellites [16]. No compensation of this lever arm was made in this basic orbit error determination. Second, the orbital force model that is assumed in the broadcast ephemeris computation is a simplification [15, A3.1.2] and neglects some of the weaker gravitational forces. Within the scope of this work, the precision of GLONASS orbit computation however seemed

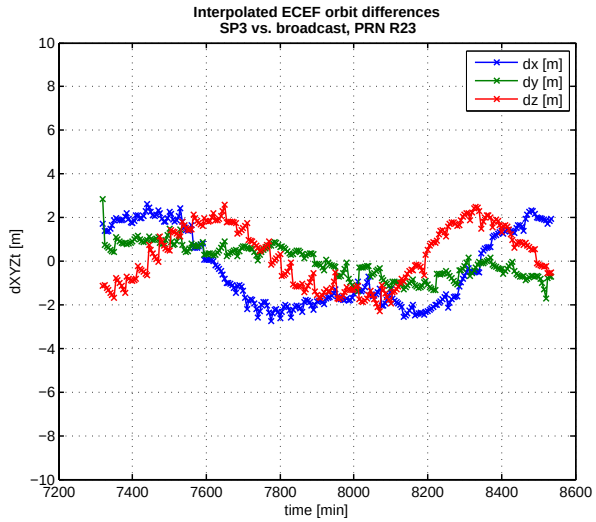

Figure 5. Orbit errors of GLONASS PRN 23

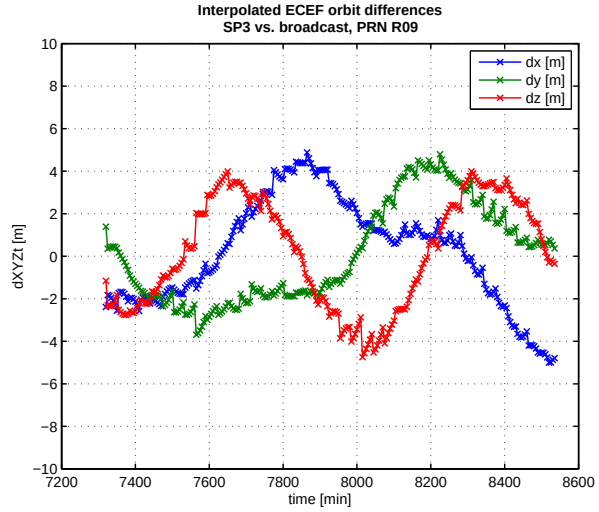

Figure 6. Orbit errors of GLONASS PRN 09

sufficient if a (one-sigma) URA of 4m is assumed. This corresponds well with the findings in [9].

2) Nominal and Integrity Biases: The biases assumed as B_{int} and B_{cont} relate to uncompensated inter-frequency biases of the satellite payloads, and variations of the phase center. These values strongly depend on the respective hardware; they are however difficult to estimate. For simplification of the high-level task we assume that the biases assumed for next-generation hardware can already be expected with the current constellation.

3) User Code Tracking Noise and Multipath: The signal structure, and also the receiver architectures for GLONASS and semi-codeless GPS P(Y) tracking suggest that both the noise level of code measurements and the magnitude of multipath biases differ from the values for L1 GPS measurements. This result is confirmed by [10] for raw range measurements in GPS L2/P(Y). However it can be shown from data analysis that the noise level of smoothed measurements can be assumed equal for GPS L1, L2 and L5 measurements. We take this assumption for GPS and also GLONASS, thus no change of the L1/L5 error model is proposed in this relation.

4) Multipath reduction due to filtering: As for the L1/L5 model, the conservative approach that assumes MOPS compliant multipath for the smoothed measurements [24] is taken. Thus no reduction of the multipath error due to smoothing is assumed.

5) Receiver noise increases due to ionosphere free linear combinations: The factor that precedes the user tracking and multipath noise if a linear combination from two frequency is formed,

$$n_{\text{iono}} = \sqrt{\frac{f_1^4 + f_2^4}{(f_1^2 - f_2^2)^2}} \quad , \tag{10}$$

has to be adapted to the GPS L1/L2 and GLONASS L1/L2 case. Fortunately the L1 and L2 channels of GLONASS are set at a specific ratio for all channel numbers:

$$\begin{aligned} f_{\text{L1,GLO}}(k) &= 1602 + k \cdot \frac{9}{16}[\text{MHz}] \\ f_{\text{L2,GLO}}(k) &= 1246 + k \cdot \frac{7}{16}[\text{MHz}] \\ \frac{f_{\text{L1,GLO}}}{f_{\text{L2,GLO}}} &= \frac{9}{7} \end{aligned} \tag{11}$$

The corresponding fixed ratio can directly be applied in the error model and is, for GPS and GLONASS L1/L2 combinations,

$$n_{\text{iono,GPS}} = \sqrt{\frac{{f_{\text{L1,GPS}}}^4 + {f_{\text{L2,GPS}}}^4}{\left({f_{\text{L1,GPS}}}^2 - {f_{\text{L2,GPS}}}^2\right)^2}} = 2.978, \tag{12}$$

and

$$n_{\text{iono,GLONASS}} = \sqrt{\frac{{f_{\text{L1,GLO}}}^4 + {f_{\text{L2,GLO}}}^4}{\left({f_{\text{L1,GLO}}}^2 - {f_{\text{L2,GLO}}}^2\right)^2}} = 2.958\ . \tag{13}$$

This concludes the adaptation of the user range error model.

D. ARAIM specific parametrization

A few parameters specific to ARAIM are presented here. They represent an average, and not too pessimistic expectation of future GNSS performance levels [8] with the limitation that no constellation faults were assumed.

- $P_{sat} = 10^-5$ [per 150s]
- $P_{const} = 0$ for simplification of the analysis.
- $P_{\text{HMI}} = 2 \cdot 10^-7$, where the entire budget is allocated into the vertical domain and horizontal integrity is neglected.

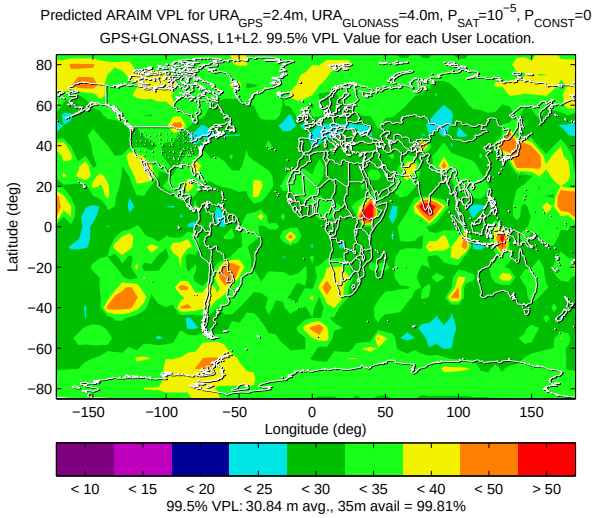

Figure 7. 99.5^{th} percentile of the VPL for the prediction of the flight experiment scenario (31 GPS+24 GLONASS). The simulation was based on a 5x5 degrees user grid during one day, at 5min intervals. GPS URA was set to 2.4m, GLONASS URA was set to 4m. Prior Fault Probability per SV and per approach is 10^{-5}. No constellation faults are assumed.

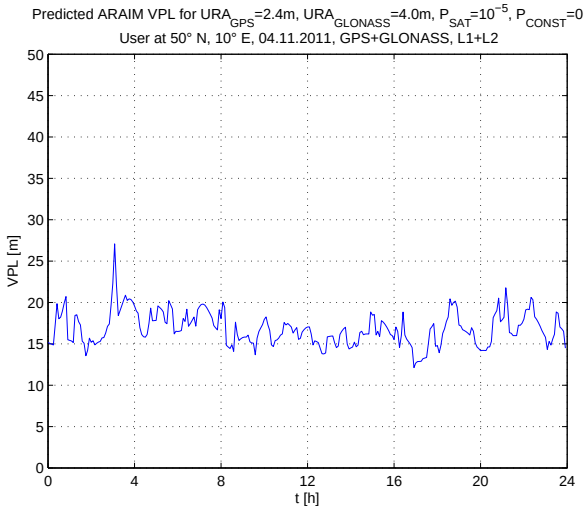

Figure 8. Predicted VPL for a user at [50°N, 10°E] during one day

E. Summary of L1/L2 error model

The modified L1/L2 dual frequency error model for ARAIM is summarized in Table II. It can be seen that apart from different URA values and the adjustment of the noise inflation factors caused by ionosphere free combinations, the dual frequency model for L1/L2 can be approximated by the L1/L5 model. In the next section this model will now be applied to ARAIM performance estimations.

IV. Predicted Performance of L1/L2 ARAIM

With the modifications from Section III it is now possible to obtain a predictive analysis of the expected ARAIM performance for the scenario. A grid simulation has been executed where the GPS and GLONASS orbits of the particular flight test day (in the form of almanac data) and the previously defined user error budget were configured. The simulation was implemented using the MAAST [18] simulation toolkit and the identical ARAIM user algorithm that was later applied in flight data processing. The user grid was set up at latitude and longitude spacing of 5 degrees around the globe, and a one-day simulation at a five minute interval was executed. All other parameters such as the elevation mask were set to the same values as in the later flight experiment.

The plot in Figure 7 shows the 99.5^{th} percentile of the VPL for each user location during the day 2011-Nov-04 on which the flight was made. For simplification we assume a constant URA of 2.40m for the GPS satellites. The impact of this simplification is minor, because only some of the satellites had URA set to a larger value during a short time period on this day.

As expected the predicted VPL level seems comparable to studies presented in [22, 8]. The availability would not provide for a perfect coverage of LPV-200 service, but the impact of the larger URA values is rather minor. Figure 8 shows the course of the actual VPL value for a grid point chosen near the Braunschweig Airport (50N / 10E). Here the difference between the worst-case 99.5^{th} percentile and the actual values becomes clear: The average performance is below 20m for this user while the worst case (the 99.5 percentile) reads 20-25 m according to the color key in Figure 7.

V. Flight Test Performance

This section presents the results from post-processing the flight trial data collected through a test flight executed on Nov 04, 2011 with DLR's research aircraft ATTAS.

A. Positioning performance during flight test

The trajectory of the flight was shown in Figure 2, and Figure 9 presents the position error of the calculated solution with respect to an RTK reference trajectory.

The respective values for the geometry size n_{SV} that could be used to compute the position is given in Figure 10. As mentioned before, several rather dynamic maneuvers had been conducted during the flight, including multiple 360-degree turns at high banking angles up to 60°. These are reflected in temporary outages of lots of satellites and a higher position error. They can be observed at multiple points through the flight test, and it can also be seen that the time until the geometry size is back at the nominal level is rather large due to long waiting times of 360s in filter convergence. The corresponding maneuvers can be seen in Figure 11. Here, the relative position of the aircraft with respect to the Airport Reference Point (ARP) is plotted.

B. Integrity analysis of the flight data

In this section we present the ARAIM vertical protection level derived from the positioning results. A limited statement about integrity can be made from the results, however it

Nominal Error	GPS L1/L2 P(Y)	GLONASS L1/L2
Orbit/Clock	Broadcast	Constant (4m)
Signal Deform., PCV & IFB	L1/L5	
Ionosphere	Neglected	
Troposphere	MOPS model [1]	
Multipath	L1/L5	
Code Tracking	L1/L5	
RX biases	L1/L5	
Smoothing	L1/L5	
Ifree Linear Combination	Adjust to f_1, f_2	

Table II
MODIFIED UERE BUDGET FOR THE GPS & GLONASS L1/L2 SCENARIO

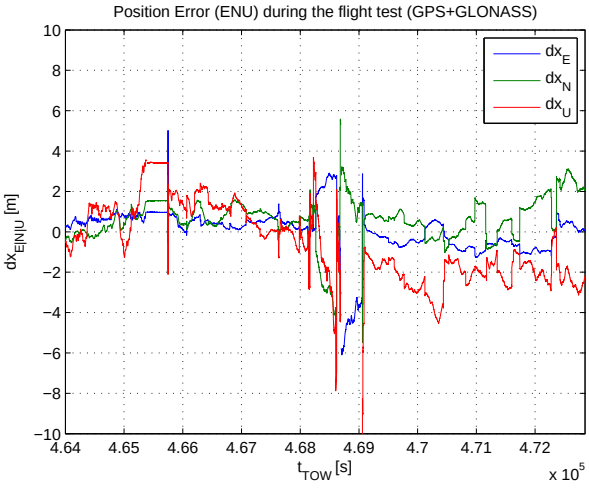

Figure 9. Local position error during flight test. The position error is given in East/North/Up coordinates.

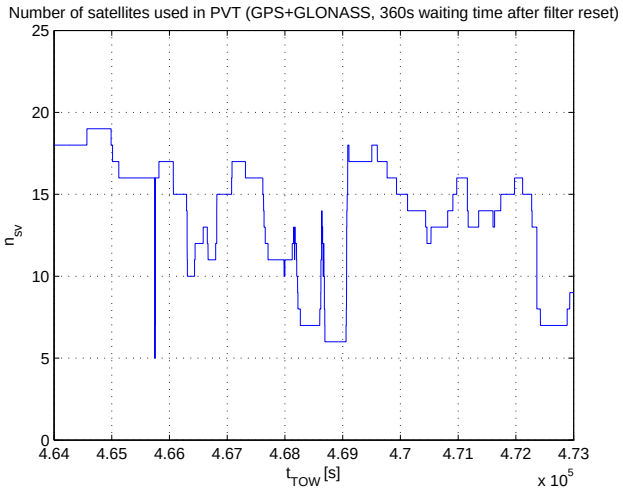

Figure 10. Number of Range Measurements used in PVT and ARAIM processing. Multiple situations with severe geometry deterioration can be observed, in particular during the first phase of the flight test that includes multiple 360-degree turns. Due to the long filter waiting time after a signal loss-of-lock the PVT solution can only slowly return to nominal operation after maneuvers including a high bank angle.

is important to state that the small number of data points collected during one single flight can not serve to prove integrity of the ARAIM implementation with respect to error bounds at a $2 \cdot 10^{-7}$ integrity risk. However the performance level with respect to availability can be seen and, given that the error model derived above is accurate, it represents a good estimate of the impact of operational factors on ARAIM performance. Of course the assumed "truth" or reference trajectory is potentially an additional error source in this analysis – it is derived from carrier phase measurements taken with the same receiver, and an RTK computation that uses ground reference data from our experimental GBAS station at the airport to obtain carrier phase level accuracy.

In Figure 12 the absolute vertical position error (blue) against the predicted, optimized [4] vertical protection level (red) is plotted. The protection level does not directly depend on data in terms that the solution separation is predicted from the URE based UERE model. However a FDE algorithm tests this prediction against the current solution separation at each epoch, and would exclude satellites if the solution separation exceeds its prediction [13, Eq. 3-6,3-7]. From the comparison of the position error magnitude and the protection level it can be seen that the latter is a valid error bound for the position error. In a single situation it can be observed that both the position error and the VPL become excessively large, obviously while performing a turn maneuver at $t \approx 4.687 \cdot 10^5 s$.

In Figure 13 a detail of the data is shown, including two of the circle maneuvers at $t \approx 468200s$ and $t \approx 468600s$. The protection level increases and still bounds the error. The cause for the large VPL follows directly from the loss of signal during those turns. The observed effect is increased by the coincidence that all previously lost measurements from the first circle return seconds before the next maneuver commences. Looking at the reference position data for the time instant (Figure 14) it appears that while flying this maneuver, the RTK reference position was lost due to a lack of visible satellites. It is important to bear in mind that around this time instant the position error might be inaccurate because it is derived from a RTK reference based on only few measurements. The maximum VPL (which is cut off in this plot for better representation of the details) can be observed at 450m, and this is clearly caused by the weak geometry. The corresponding time instant can be clearly seen in the number of considered satellites, where the number of range measurements drops to only 6 satellites. With 5 measurements

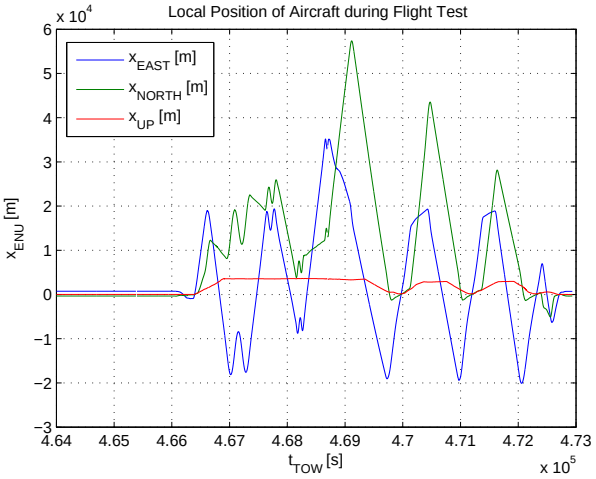

Figure 11. Local Position of Aircraft during Flight Test (Position vs. Airport Reference Point ARP). The first phase of flight includes multiple full circle maneuvers flown at an altitude of 12.000ft. After $t = 4.69s$ the aircraft performs three instrumental approaches to EDVE Runway 08 with a low pass at approx. 400ft AGL. After the last pass a visual traffic circuit and a full stop landing are performed.

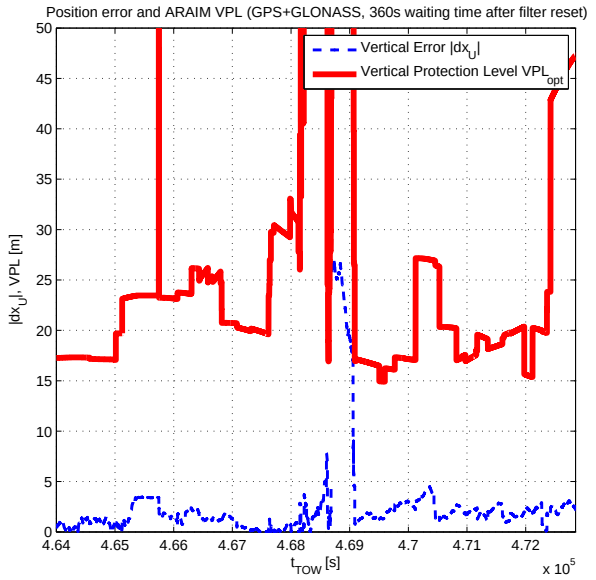

Figure 12. Vertical Position Error and Vertical Protection Levels

already necessary to compute a position including two system times, 6 visible satellites constitute the absolute minimum to perform RAIM/ARAIM and this is reflected in the high VPL obtained.

The turn maneuvers however do not represent very likely approach patterns, even in future. Holdings and late turn-to-final curves however are realistic scenarios, and they can also include bank angles that are large enough to remove a significant part of the available measurements. With the standard duration of a holding pattern being 4 minutes, any loss of signal occurring during such an operation may still have

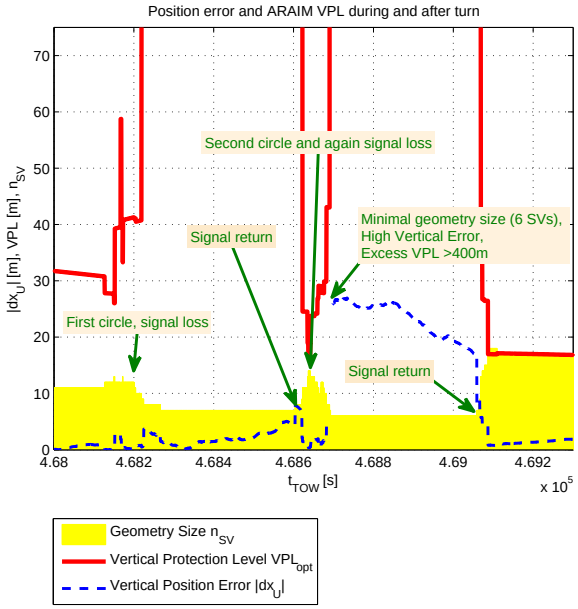

Figure 13. Geometry size, VPL and vertical error during two turn maneuvers flown with a 6 minutes level flight segment in between. Due to the long filter convergence time the position estimate is based on 7 SVs for the entire level flight segment after the first circle element. Just as the filters have converged and more measurements become available, the second 360° maneuver begins. While a momentary decrease of both position error and VPL can be seen while the maneuver starts, the geometry drops down to only 6 measurements at the end of the second circle. The VPL and vertical error increase dramatically and stay large for several more minutes, until the filters have again converged.

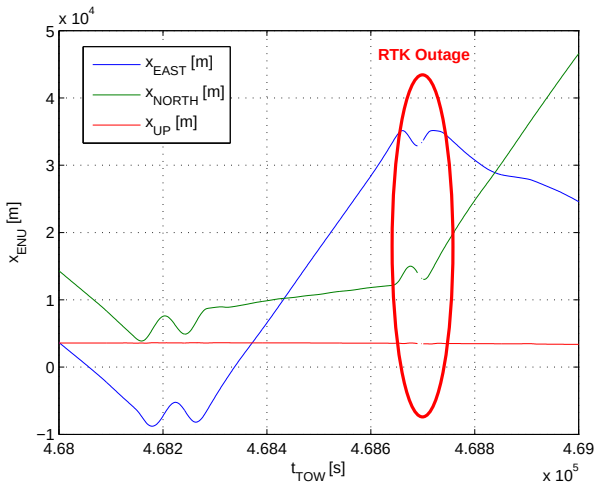

Figure 14. Reference position during the turn maneuver

an impact during the final approach segment for example. In the following we therefore concentrate on the second half of the flight which contained multiple instrument approaches and a visual circuit with a much shorter final leg at the very end.

Figure 15 is the top-down view of this phase. It starts after the very small 360° turns that was previously analyzed, and includes three low passes above runway 08 at approximately 400ft AGL, then followed by a visual circuit and a full-stop

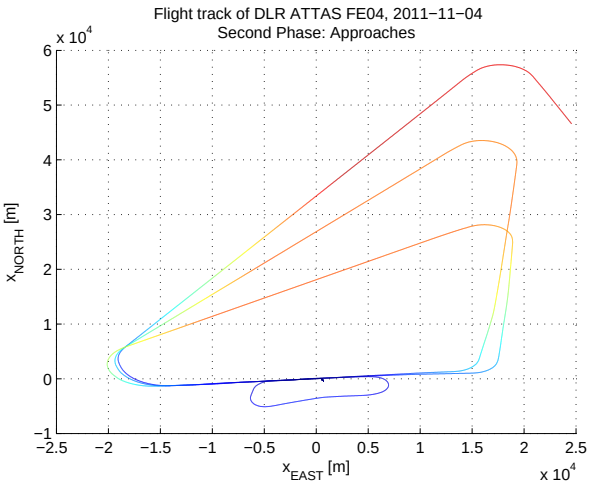

Figure 15. Flight track during approaches

landing. The detail of the Vertical Protection Level (VPL) plot in Figure 16 gives the performance level reached during level flight and occasional turns. In general no large performance gaps can be observed while the plane performs its approaches and departures, however during the more dynamic phase at the end of the flight, where a visual traffic circuit was flown, ARAIM fails again due to the small geometry.

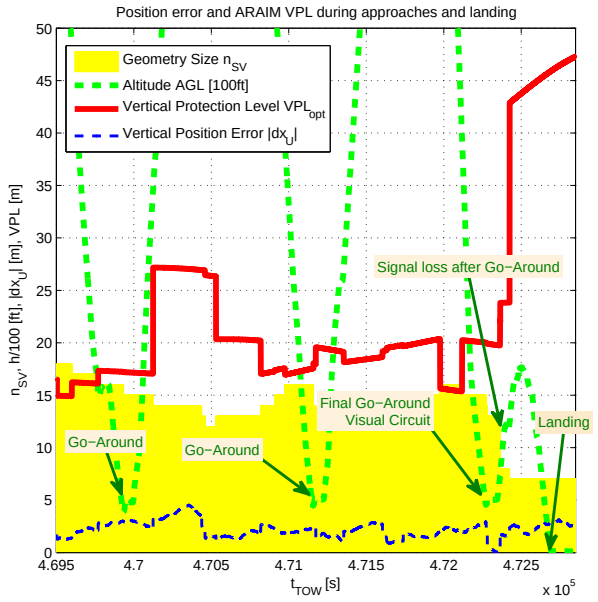

Figure 16. Geometry Size, Aircraft Altitude, VPL and vertical error during four approaches including the landing. During the "IFR" approaches with wider turns no severe performance impairment is observed. However after the last go-around while turning to a visual downwind segment, the geometry size drops again below 10 SVs, and the corresponding VPL grows.

C. GPS-only performance

For comparison, the second part of the flight trial is analyzed with only the GPS measurements utilized. Figure 17 shows the GPS-only results with solid lines and the previously shown results from GPS and GLONASS as dashed lines. As expected the VPL for a single-constellation scenario is significantly larger during the flight. The vertical error component is in the same value range. Note that the signal loss scenario towards the final landing obviously affected all GLONASS satellites: The VPL for both scenarios is the same. Two of ten visible GPS satellites were also lost.

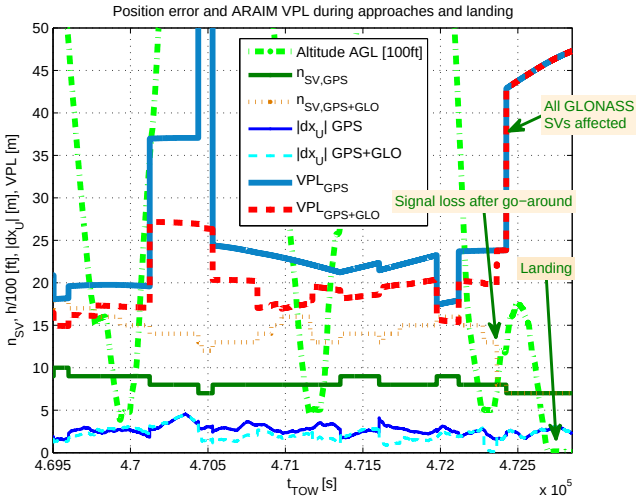

Figure 17. Geometry Size n_{SV}, Aircraft Altitude, VPL and vertical error $|dx_u|$ using GPS only (solid lines). Dashed lines show previous multi-constellation results for comparison. As expected, the vertical protection level is larger when only one GNSS is used. The magnitude of the vertical position error is however not significantly enlarged. In the last minute it can be observed that the previously identified loss of signals affected all GLONASS satellites, thus the resulting VPL is identical with that of the combined constellation scenario.

D. Comparison with ARAIM prediction

We now compare the results obtained from a prediction of ARAIM performance with the actual data derived from the flight campaign. As can be seen in Figure 18, the "baseline" level of VPL in the flight test fits well the predicted VPLs for a single user at position $50°\text{N}, 10°\text{E}$. Whenever maneuvers including high bank angles are flown however, a significantly increased VPL is observed. It can be seen from the geometry size plot in Figure 10 that this increase is directly caused by blocking of some of the signals during the respective turns. In addition to direct blocking, a guard time of 360s will be added for each channel to allow for filter convergence – this effectively extends the impact of any signal loss occurring *during* one maneuver to as long as the subsequent 6 minutes *after* the maneuver.

If the filter convergence could be accelerated by taking into account information coming from satellite measurements without interruption, or INS aiding, the impact of such signal loss could potentially be reduced. In the following analysis

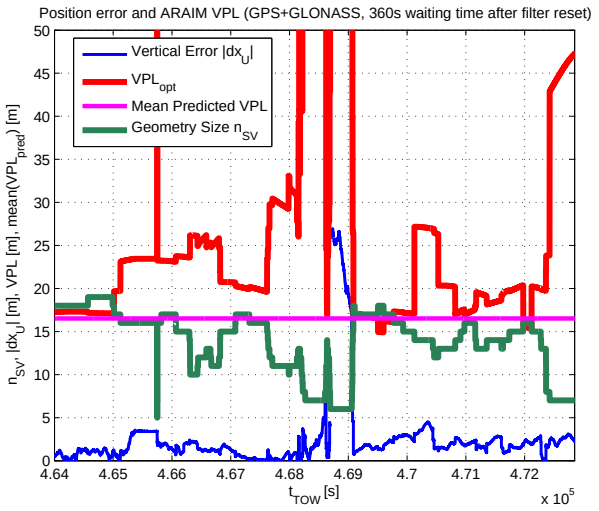

Figure 18. Vertical Protection Level obtained during flight test compared with the average predicted VPL for the given day, both based on identical UERE assumptions. The effect of geometry degradation can be directly seen from the development of the geometry size and the actual VPL during the maneuvers.

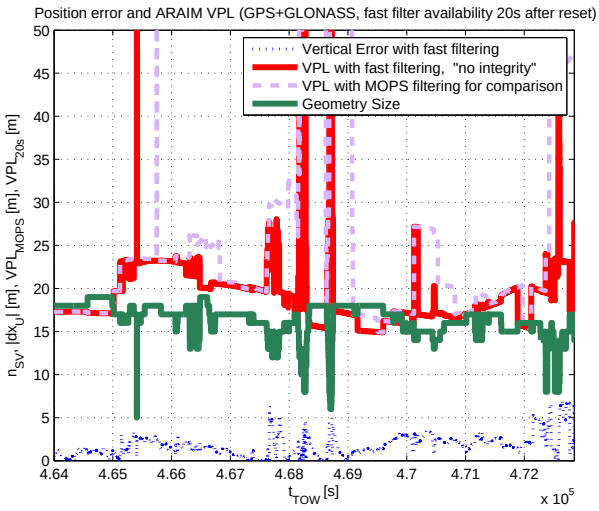

Figure 19. Geometry Size n_{SV}, Aircraft Altitude, VPL and vertical error $|dx_u|$ assuming that filtered measurements can be used only 20s after the filter starts running. Note that it can not be safely assumed that the Vertical Protection Level bounds the vertical error in this case, because the necessary properties of the filtered range measurements are not assured. The dashed line depicts the VPL obtained with MOPS compliant filtering.

in Figure 19 the PVT data processing has been modified to accept measurements already 20s after the filter starts smoothing when the respective satellite channel has re-gained lock. Of course the error model for receiver tracking noise and multipath from Section III does not hold here, so overbounding of the position error can not be trusted and is denoted "no integrity" in the plot. What comes as a surprise is that the position error directly after resuming navigation is quite small, and compared with the results in Figure 12, it is even smaller. The exceedingly small geometries in the case with long filter waiting times have introduced large errors that are not present here.

Concerning the availability of ARAIM integrity it can be seen in this hypothetical situation that any means of reducing the "time to first fix" after signal loss can greatly improve operational performance for aircraft executing dynamic maneuvers before they attempt to land. It has to be made sure however that these methods do not invalidate the user ranging error model, in particular the assumed property of zero-mean noise for the smoothed range tracking and multipath error.

VI. Conclusion

As was shown, ARAIM can already be demonstrated with L1/L2 data in realistic flight scenarios at a performance level that is at least promising with respect to LPV-200 operations. However several severe performance drops could be observed during turn maneuvers in the flight trial. Due to the necessary waiting time until smoothing filters converge after a reset, each signal loss during a turn maneuver implies a certain period where only a reduced geometry is available. Moreover multiple signal losses that otherwise would occur at different times can add up and lead to very weak geometries, in particular when full circles are flown. Finally, the L2 band is not usable as an ARNS band, which necessitates the update of at least two GNSS constellations to provide L1 and L5 signals in order to arrive at the performance level demonstrated here.

As a preparative measure for processing the data, it has been found that accurate definition of the User Equivalent Range Error (UERE) model parameters is crucial to obtain a meaningful result on ARAIM performance. While some of the error budget contributions can safely be assumed identical in L1/L5 scenarios and in the present L1/L2 scenario, other parts of the model have to be adjusted. This includes the use of semi-codeless P(Y) tracking for GPS, and in general the use of GLONASS as a GNSS that is not considered in the L1/L5 assumptions for future ARAIM applications. An analysis of the GPS and GLONASS orbit errors has been conducted based on broadcast orbits and precise ephemeris products from the IGS. The results for GPS suggest that the broadcast URA value can be used to model the ephemeris and clock errors. Although the broadcast values are usually much larger than the expectation for future GNSS, the impact on the ARAIM performance is not exceedingly strong. For GLONASS a value of 4.00 m has proven as a good estimate for URA. However extensive analysis would be necessary to obtain a high enough confidence level for this value to safely use it in an actual integrity frame.

Another finding of the analysis was that modulation related error contributions do not differ significantly when smoothed ranges are considered. Thus, the MOPS [24] models for tracking noise and multipath errors can be applied to L2/P(Y) signals, and also for GLONASS measurements.

In summary it can be recorded that the modeled performance of ARAIM can be confirmed with flight data if the flight state is steady and good conditions for GNSS signal reception

are given. The set of currently available L1 and L2 signals and the precision of the broadcast GPS and GLONASS orbits are sufficient to provide rather good ARAIM availability, but the robustness of the latter URA estimates has to be matched with its requirements for LPV-200 compliant ARAIM. Also a stringent proof of integrity would require much more data than from a single flight experiment, and a highly reliable position reference system.

Maneuvering of the aircraft including banking can significantly reduce the ARAIM performance however. It is obvious that these limitations will still have a large impact in future L1/L5 scenarios. The availability loss during the final phases of a flight can be critical and are aggravated by the fact that MOPS smoothing filters require a long time to recover after a loss of lock. This finding has to be accounted for in predictions of future ARAIM performance, and a solution to moderate the performance impact of maneuvering has to be found for the airborne algorithm.

ACKNOWLEDGMENT

The authors thank their colleagues at DLR and the experts in the WG-C ARAIM subgroup for many interesting and insightful discussions on ARAIM and future ISM architectures. Many thanks goes in particular to Dr. Oliver Montenbruck from the German Space Operations Center (GSOC) who could successfully help understanding of some of the not-so-keplerian details of GLONASS orbit computation.

REFERENCES

[1] *Airborne Supplemental Navigation Equipment Using the Global Positioning System (GPS), Technical Standard Order (TSO), C-129*. U.S. Federal Aviation Administration, Washington, D.C., 1992.

[2] Bilateral EU-US ARAIM Technical Sub Group of the Working Group C. *GPS-Galileo Working Group C ARAIM Technical Subgroup Interim Report (Issue 1.0, 19 December 2012)*. Tech. rep. Bilateral EU-US ARAIM Technical Sub Group of the Working Group C, 2012.

[3] Bilateral EU-US ARAIM Technical Sub Group of the Working Group C. *GPS-Galileo Working Group C ARAIM Technical Subgroup Milestone IIA Report (Draft 2, 2013)*. Tech. rep. Bilateral EU-US ARAIM Technical Sub Group of the Working Group C, 2013.

[4] Juan Blanch, Alexandru Ene, Todd Walter, and Per Enge. "An Optimized Multiple Hypothesis RAIM Algorithm for Vertical Guidance". In: *Proceedings of the ION GNSS 2007 Conference*. 2007.

[5] Juan Blanch, Todd Walter, and Per Enge. "RAIM with Optimal Integrity and Continuity Allocations Under Multiple Failures". In: *IEEE Transactions on Aerospace and Electronic Systems* 46.3 (July 2010), pp. 1235–1247.

[6] Juan Blanch, Todd Walter, Per Enge, Young Lee, Boris Pervan, Markus Rippl, and Alexandru Spletter. "Advaced RAIM User Algorithm Description: Integrity Support Message Processing, Fault Detection, Exclusion, and Protection Level Calculation". In: *ION Institute of Navigation Global Navigation Satellite Systems Conference*. 2012. URL: http://elib.dlr.de/81070/.

[7] Juan Blanch, Todd Walter, Per Enge, Stefan Wallner, Francisco Amarillo Fernandez, Riccardo Dellago, Rigas Ioannides, Ignacio Fernandez Hernandez, Boubeker Belabbas, Alexandru Spletter, et al. "Critical Elements for a Multi-Constellation Advanced RAIM". In: *Navigation* (2013).

[8] Juan A. Blanch, Todd F. Walter, Per K. Enge, Stefan Wallner, Francisco Amarillo Fernandez, Riccardo Dellago, Rigas Ioannides, Boris Pervan, Ignacio Fernandez Hernandez, Boubeker Belabbas, Alexandru Spletter, and Markus Rippl. *A Proposal for Multi-Constellation Advanced RAIM for Vertical Guidance*. 2011. URL: http://elib.dlr.de/75016/.

[9] Myungjun Choi, Juan Blanch, Dennis Akos, Liang Heng, Grace Gao, Todd Walter, and Per Enge. "Demonstrations of Multi-constellation Advanced RAIM for Vertical Guidance Using GPS and GLONASS Signals". In: *Proceedings of the 24th International Technical Meeting of the Satellite Division of The Institue of Navigatoin - ION GNSS*. 2011.

[10] M.-S. Circiu, M. Felux, P. Remi, L. Yi, B. Belabbas, and S. Pullen. "Evaluation of Dual Frequency GBAS Performance using Flight Data". In: *Proceedings of the International Technical Meeting of the Institue of Navigation (ITM2014)*. 2014.

[11] Alexandru Ene, Juan Blanch, and Todd Walter. "Galileo-GPS RAIM for Vertical Guidance". In: *Proceedings of the Institute of Navigation's National Technical Meeting, Monterey CA*. 2006.

[12] FAA GEAS Panel. *GNSS Evolutionary Architecture Study: Phase I - Panel Report*. Report. GNSS Evolutionary Architecture Study Panel, 2008. URL: http://www.faa.gov/about/office_org/headquarters_offices/ato/service_units/techops/navservices/gnss/library/documents/media/GEAS_PhaseI_report_FINAL_15Feb08.pdf.

[13] FAA GEAS Panel. *Phase II of the GNSS Evolutionary Architecture Study*. Report. GNSS Evolutionary Architecture Study Panel, Feb. 2010. URL: http://www.faa.gov/about/office_org/headquarters_offices/ato/service_units/techops/navservices/gnss/library/documents/media/GEASPhaseII_Final.pdf.

[14] M. Fritsche, R. Dietrich, C. Knöfel, A. Rülke, S. Vey, M. Rothacher, and P. Steigenberger. "Impact of higher-order ionospheric terms on GPS estimates". In: *Geophysical Research Letters* 32.23 (2005), n/a–n/a. ISSN: 1944-8007. DOI: 10.1029/2005GL024342. URL: http://dx.doi.org/10.1029/2005GL024342.

[15] *GLONASS Interface Control Document L1,L2*. Russian Institute of Space Device Engineering, 2008.

[16] Liang Heng, Grace Xingxin Gao, Todd Walter, and Per Enge. "Statistical Characterization of GLONASS Broadcast Clock Errors and Signal-In-Space Errors". In: *Proceedings of the 2012 International Technical Meeting of the Institute of Navigation (ION ITM 2012), Newport Beach, CA*. 2012, pp. 1697–1707.

[17] International Civil Aviation Organization (ICAO). *Annex 10, Aeronautical Telecommunications, Volume I (Radio Navigation Aids)*. International Civil Aviation Organization, 2005.

[18] S. Jan, W. Chan, T. Walter, and P. Enge. "Matlab Simulation Toolset for SBAS Availability Analysis". In: *Proceedings of the ION GNSS Conference 2001*. 2001.

[19] Gary A. McGraw, Tim Murphy, Mats Brenner, Sam Pullen, and A. J. Van Dierendonck. "Development of the LAAS Accuracy Models". In: *ION GPS*. 2000.

[20] Boris S. Pervan, Samuel P. Pullen, and Jock R. Christie. "A Multiple Hypothesis Approach to Satellite Navigation Integrity". In: *Journal of The Institute of Navigation* 45.1 (1998).

[21] Markus Rippl. "Real Time Advanced Receiver Autonomous Integrity Monitoring in DLR's Multi-Antenna GNSS Receiver". In: *International Technical Meeting of the Institue of Navigation (ITM2012)*. 2012. URL: http://elib.dlr.de/74985/.

[22] Markus Rippl, Alexandru Spletter, and Christoph Günther. "Parametric Performance Study of Advanced Receiver Autonomous Integrity Monitoring (ARAIM) for Combined GNSS Constellations". In: *ION 2011 International Technical Meeting*. 2011. URL: http://elib.dlr.de/69128/.

[23] *RTCA/DO-208: Minimum Operational Performance Standards for Airborne Supplemental Navigation Equipment Using Global Positioning System (GPS)*. RTCA Special Committee 159, 1991.

[24] *RTCA/DO-229D: WAAS Minimum Operational Performance Specification (MOPS)*. RTCA Special Committee 159, 1991.

[25] Todd Walter and Per Enge. "Weighted RAIM for Precision Approach". In: *Proceedings of the ION GNSS Conference 1995*. ION. 1995. URL: http://waas.stanford.edu/papers/wraim_tfw95.pdf.